Effects of Acetylcholine Release Spatial Distribution on the Frequency of Atrial Reentrant Circuits: a Computational Study.

Chiara Celotto[1,2], Carlos Sánchez[1,2], Mostafa Abdollahpur[3], Frida Sandberg[3], Jose F. Rodriguez[4], Pablo Laguna[1,2], Esther Pueyo[1,2]

[1] Aragon Institute of Engineering Research, University of Zaragoza, IIS Aragón, Zaragoza, Spain
[2] CIBER in Bioengineering, Biomaterials and Nanomedicine, Zaragoza, Spain
[3] University of Lund, Lund, Sweden
[4] Politecnico di Milano, Milano, Italy

Abstract

The frequency of the ECG fibrillatory f-waves (F_{f}) in atrial fibrillation (AF) shows significant variations over time. Cardiorespiratory interactions through the autonomic nervous system have been suggested to play a role in such variations. Here, we tested whether the spatial distribution associated with the release of the parasympathetic neurotransmitter acetylcholine (ACh) could affect the frequency of atrial reentrant circuits.

Computational simulations in a human persistent-AF 3D atrial model were performed. We evaluated two different patterns of atrial innervation: ACh release restricted to the area of the ganglionated plexi (GP) and the nerves departing from them, following the so-called octopus hypothesis, and ACh release distributed uniformly randomly throughout the atria. In both cases, ACh release sites occupied 8% of the atria. The temporal pattern of ACh release was simulated following a sinusoidal waveform of frequency 0.125 Hz (respiratory frequency). Different mean levels and peak-to-peak variation ranges of ACh were tested.

We found that variations in the dominant frequency F_{f} followed the simulated temporal ACh pattern in all cases, with F_{f} modulation being more pronounced for increasingly larger ACh variation ranges. For the tested percentage of ACh release sites (8%), the spatial distribution of ACh did not have an impact on F_{f} modulation.

1. Introduction

The autonomic nervous system (ANS) has been reported to be involved in the genesis and maintenance of atrial fibrillation (AF) [1]. Sympathetic activation acts as a trigger by facilitating the genesis of ectopic beats. Parasympathetic hyperactivity facilitates the formation of reentries by shortening the wavelength of reentry, defined as the distance traveled by the depolarization wave during the effective refractory period. The cardiac ANS is divided into its extrinsic and intrinsic components, with the intrinsic one being organized in a network of interconnecting axons and clusters of autonomic ganglia called ganglionated plexi (GPs).

Chaotic electrical activation during AF is reflected in the electrocardiogram (ECG) in a series of waves known as f-waves, whose frequency (F_{f}) shows significant variations over time. Cardiorespiratory interactions through the ANS have been suggested to play a role in F_{f} modulation. In particular, a reduction in F_{f} modulation after full vagal blockade by atropine injection has been reported [2].

We used computational modeling and simulation to evaluate F_{f} modulation as a function of the spatio-temporal release pattern of acetylcholine (ACh), the primary neurotransmitter of the parasympathetic nervous system. Whole-atria models representative of persistent AF (psAF) were built. Different spatial distributions of ACh release sites were simulated to evaluate their effects in the mean ($\overline{F_{\mathrm{f}}}$) and range ($\Delta F_{\mathrm{f}}$) of F_{f} [3]. Simulation results were compared with the results from clinical data analysis [3].

2. Methods

2.1. Clinical recordings

Our modeling and simulation study aimed at reproducing the conditions evaluated in the clinical study reported in [3], where modulation of F_{f} by respiration through the parasympathetic nervous system was investigated. In a group of seven psAF patients, resting ECGs were recorded at baseline (spontaneous respiration), during 0.125 Hz frequency-controlled respiration and during controlled respiration after full vagal blockade by atropine injection.

Table 1. $\overline{F_{\mathrm{f}}}$ and ΔF_{f} in simulations and patients.

SIMULATIONS										EXPERIMENTS	
		$\mathcal{O}_{08}$			$\mathcal{D}_{08}$			**Mean values from simulation**		**Mean values from patients**	
ACh release 0.125 Hz		**Range of ACh**			**Range of ACh**						
Mean ACh		**0.0**	**0.05**	**0.1**	**0.0**	**0.05**	**0.1**				
0.05 μM	$\overline{F_{\mathrm{f}}}$	7.69	7.66	7.66	7.43	7.42	7.63	$\overline{F_{\mathrm{f}}}$	7.59	$\overline{F_{\mathrm{f}}}$	6.82
	ΔF_{f}	0.00	0.01	0.11	0.00	0.01	0.08	σ	0.12	σ	0.59
	r		0.45	0.80		0.46	0.72				
0.075 μM	$\overline{F_{\mathrm{f}}}$	7.43	7.73	not tested: out of phy. range	7.51	7.76	not tested: out of phy. range	ΔF_{f}	0.025	ΔF_{f}	0.15
	ΔF_{f}	0.01	0.02		0.00	0.01		σ	0.035	σ	0.01
	r		0.47			0.59					

2.2. Atrial models

Human atrial electrical activity was simulated in a 3D bi-atrial anatomical model that included detailed regional descriptions of fiber direction and functional heterogeneity [4].

The electrophysiological behavior of atrial myocytes was described by the Courtemanche human atrial action potential (AP) model [5], which was subsequently adapted to represent atrial heterogeneities in different regions by modifying the current conductances as in [4]. To account for parasympathetic effects, we introduced the formulation of the ACh-activated potassium current, I_{KACh}, developed by Kneller [6] and updated by Bayer [7]. Electrical remodeling associated with psAF was modeled by reducing the conductances of I_{to}, I_{CaL} and I_{kur} by 50%, 70% and 50%, respectively, and by increasing the conductance of I_{K1} by 100%, as in [8]. Structural remodeling induced by psAF was simulated by including 20% diffuse fibrosis based on histological studies reporting diffuse fibrosis percentages up to 40%, with a mean of approximately 20%, in psAF patients [9]. We uniformly randomly selected 20% of the tissue nodes and we assigned them the MacCannell fibroblast computational AP model [10].

Tissue conductivities in different atrial regions were defined according to the values reported in [4]. The conductivity betweeen fibroblasts or between myocytes and fibroblasts was reduced 4-fold with respect to the myocyte-myocyte coupling. The total activation time (TAT) in our simulations was 180 ms, in line with experimental results reported in the literature for psAF patients [11].

2.3. Simulated ACh release patterns

To realistically represent the heterogeneous ACh release in the atria, we modeled the GP location following the anatomical study by Armour et al. [12]. The following 5 major GPs were considered: the superior right atrial GP (SRA-GP); the superior left atrial GP (SLA-GP); the posterior right atrial GP (PRA-GP); the posteromedial left atrial GP (PMLA-GP) and the posterolateral left atrial GP (PLLA-GP), illustrated in Fig. 1, panel A). Furthermore, to take into account autonomic nerves communicating the GPs with atrial tissue, we adopted the octopus configuration [13], with 8% of tissue nodes globally selected to be ACh release nodes. To test the effect of the heterogeneity in the organization of ACh release, we built another 3D model in which 8% of tissue nodes were uniformly randomly selected as ACh sites all over the atria. These two spatial configurations of ACh release were denoted as $\mathcal{O}_{08}$ and $\mathcal{D}_{08}$, respectively, and are represented in Fig. 1, panels A) and B).

In the selected nodes, the temporal pattern of ACh release was simulated as cyclically varying following a sinusoidal waveform of frequency equal to the 0.125 Hz respiratory frequency of the clinical recordings. Different mean levels (0.05, 0.075 μM) and peak-to-peak variation ranges (0.0, 0.05, 0.1 μM) of ACh were tested, all within ACh ranges tested in preceding studies (0 - 0.1 μM) [7].

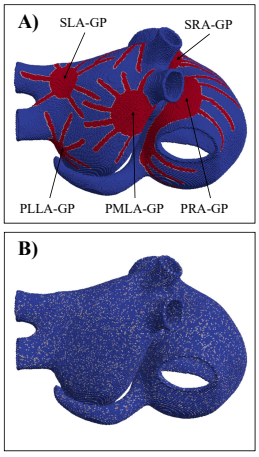

Figure 1. 3D atrial models, with ACh release nodes shown in red. A) $\mathcal{O}_{08}$ spatial configuration of ACh release, with identification of the modeled GPs. B) $\mathcal{D}_{08}$ spatial configuration of ACh release.

2.4. Numerical methods and simulations

Electrical propagation in the atria was described by the monodomain model and solved by means of the finite element method in combination with the operator splitting numerical scheme using the software ELVIRA [14].

Single cells were paced at a fixed cycle length (CL) of 800 ms for 16 minutes to reach steady-state. The steady-state values of the cellular models' state variables were used for initialization of the multi-cellular models.

Fourteen stimuli at a CL of 800 ms were applied in the region of the sinus node before delivering the stimuli according to the S1-S2 protocol for arrhythmia generation. The S1 stimulus was applied on a line joining the region between the superior and inferior left PVs and the region between the superior and inferior right PVs. The S2 stimulus was subsequently applied parallel to the S1, starting from the inferior left PV and covering only half of the S1 line length. After delivery of the S1 stimulus, the simulations were run for 12.5 s.

2.5. Dominant frequency characterization

From the simulations, voltage time series were extracted from 223 points manually selected to be approximately uniformly distributed across the tissue. For each of the extracted points, the time instant $t_{m,i}$ correspondent to the maximum upstroke velocity of beat i was determined and the instantaneous frequency was computed as $1/(t_{m,i+1} - t_{m,i})$, for all beat indices i in the recording. Next, averaging was performed over all selected points in space to compute the tissue dominant frequency F_{f} along time, as follows. First, the time series of instantaneous frequencies calculated for each tissue point were subjected to power spectral analysis. Spectral "peak-conditioned" selection was performed as in [15] so that the series whose spectrum was not sufficiently peaked were discarded. F_{f} was eventually computed as the mean of the remaining time series. Finally, $\overline{F_{\mathrm{f}}}$ was computed as the average value of F_{f}, while ΔF_{f}, the magnitude of f-wave frequency modulation, was computed as the median of the upper envelope of the bandpass-filtered F_{f} signal [3].

3. Results and Discussion

In the 3D atrial models, with both the $\mathcal{O}_{08}$ and the $\mathcal{D}_{08}$ spatial configurations of ACh release, the applied S1-S2 protocol was able to generate multiple stable rotors. The atrial dominant frequency followed in all cases the induced ACh patterns (Fig. 2), with Pearson correlation coefficient values r above 0.7227 and 0.4558 for the 0.1 μM and 0.05 μM peak-to-peak ACh ranges, respectively.

Table 1 shows $\overline{F_{\mathrm{f}}}$ and ΔF_{f} for each of the simulated cases. ΔF_{f} was found to be dependent on the ACh variation range, increasing with it. The spatial distribution of ACh release did not have significant effects on ΔF_{f} when all other factors were kept constant. Regarding $\overline{F_{\mathrm{f}}}$, we found our results to highly vary depending on the fibrillatory patterns generated in the 3D models, with 1 to 3 stable rotors found in the different simulated cases. In a previous 2D study where we analyzed the behavior of a single rotor [16], we found $\overline{F_{\mathrm{f}}}$ to be dependent on the mean ACh level. Here, we observed that when the fibrillatory patterns in the 3D models were similar to one another, our results were concordant with those in 2D tissues, with $\overline{F_{\mathrm{f}}}$ increasing with the mean ACh level. Furthermore, as expected, we noticed an increase in the dominant f-wave frequency with the number of stable rotors in the atria. The different spatial distributions of ACh release, i.e. $\mathcal{O}_{08}$ and $\mathcal{D}_{08}$ configurations, did not cause significant variation in terms of $\overline{F_{\mathrm{f}}}$ and did not seem to be correlated to the induced fibrillatory pattern.

The comparison of the mean values and standard deviations of $\overline{F_{\mathrm{f}}}$ and ΔF_{f} from simulations and from patients are reported in Table 1. In all patients, ECGs showed an f-wave frequency modulation. In 57% of the patients, this modulation was significantly reduced after atropine-induced parasympathetic inhibition, while in the rest of patients no changes were observed. When comparing simulated and clinical results, mean $\overline{F_{\mathrm{f}}}$ was approximately 1 Hz higher in the simulations, while ΔF_{f} was higher in the patients. Different conduction velocity, mean ACh level and fibrillatory pattern could contribute to explain the differences in mean $\overline{F_{\mathrm{f}}}$ between simulated and clinical data. The range of variation in ACh and the percentage of ACh release sites along the atria could explain the differences in mean ΔF_{f} between simulations and patients. Future studies could further investigate the impact of all these factors on $\overline{F_{\mathrm{f}}}$ and ΔF_{f}.

4. Conclusions

The temporal evolution of ACh release could be an important factor in f-wave frequency modulation. The spatial configuration of ACh release sites has, however, minor impact on f-wave frequency modulation. Further studies will help to fully elucidate the contribution of ACh and other factors to f-wave characteristics, which might be largely dependent on the fibrillatory pattern.

Acknowledgments

This work was supported by projects PID2019-105674RB-I00 and PID2019-104881RB-I00 (Spain), ERC-StG 638284 (ERC), ITN grant 766082 MY-ATRIA (EU) and by European Social Fund (EU) and DGA through project LMP94_21 and BSICoS group T39_20R.

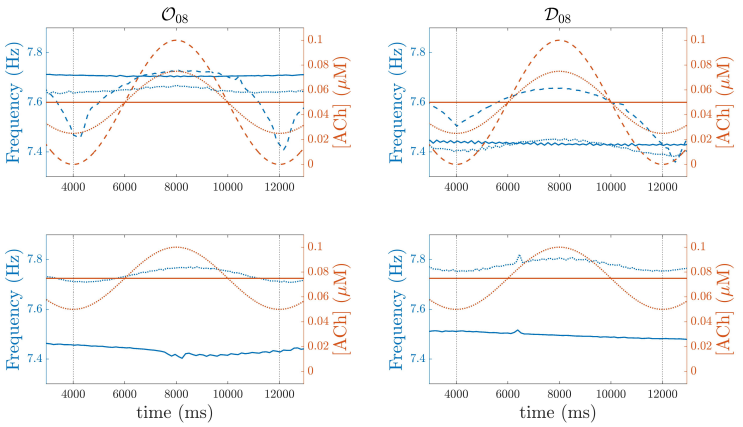

Figure 2. F_{f} (blue) for the two spatial ACh configurations, $\mathcal{D}_{08}$ and $\mathcal{O}_{08}$, following application of the S1-S2 protocol and temporal sinusoidal ACh release patterns (red). Mean ACh is 0.05 μM in the first row and 0.075 μM in the second row. Solid/dashed/dotted lines represent 0/0.05/0.1 μM ACh variation ranges. In the bottom panels, the maximum ACh variation range of 0.1 μM is not represented since it leads to ACh values out of physiological ranges. In all the panels, the two dashed vertical lines delimit one 8 second-respiratory period.

References

[1] Chang HY, et al. Effect of Vagotomy on the Activity of Cardiac Autonomic Ganglia: Insight from Left Atrial High Density Frequency Mapping. International Journal of Cardiology October 2016;220:435–439. ISSN 01675273.

[2] Holmqvist F, et al. Rapid Fluctuations in Atrial Fibrillatory Electrophysiology Detected during Controlled Respiration. American Journal of Physiology Heart and Circulatory Physiology August 2005;289(2):H754–H760. ISSN 0363-6135, 1522-1539.

[3] Abdollahpur M, et al. Respiratory Modulation in Permanent Atrial Fibrillation. In 2020 Computing in Cardiology, volume 47. December 2020; 1–4.

[4] Ferrer A, et al. Detailed Anatomical and Electrophysiological Models of Human Atria and Torso for the Simulation of Atrial Activation. PloS One 2015;10(11):e0141573. ISSN 1932-6203.

[5] Courtemanche M, et al. Ionic Mechanisms Underlying Human Atrial Action Potential Properties: Insights from a Mathematical Model. American Journal of Physiology Heart and Circulatory Physiology July 1998;275(1):H301–H321. ISSN 0363-6135, 1522-1539.

[6] Kneller J, et al. Cholinergic Atrial Fibrillation in a Computer Model of a Two-Dimensional Sheet of Canine Atrial Cells With Realistic Ionic Properties. Circulation Research May 2002;90(9). ISSN 0009-7330, 1524-4571.

[7] Bayer JD, et al. Acetylcholine Delays Atrial Activation to Facilitate Atrial Fibrillation. Frontiers in Physiology September 2019;10:1105. ISSN 1664-042X.

[8] Courtemanche M. Ionic Targets for Drug Therapy and Atrial Fibrillation-Induced Electrical Remodeling: Insights from a Mathematical Model. Cardiovascular Research May 1999;42(2):477–489. ISSN 00086363.

[9] McDowell KS, et al. Virtual Electrophysiological Study of Atrial Fibrillation in Fibrotic Remodeling. PLOS ONE February 2015;10(2):e0117110. ISSN 1932-6203.

[10] MacCannell K, et al. A Mathematical Model of Electrotonic Interactions between Ventricular Myocytes and Fibroblasts. Biophysical Journal June 2007;92(11):4121–4132. ISSN 00063495.

[11] Wesselink R, et al. Does Left Atrial Epicardial Conduction Time Reflect Atrial Fibrosis and the Risk of Atrial Fibrillation Recurrence after Thoracoscopic Ablation? Post Hoc Analysis of the AFACT Trial. BMJ open March 2022; 12(3):e056829. ISSN 2044-6055.

[12] Armour JA, et al. Gross and Microscopic Anatomy of the Human Intrinsic Cardiac Nervous System. The Anatomical Record February 1997;247(2):289–298. ISSN 0003-276X.

[13] Zhou J, et al. Gradients of Atrial Refractoriness and Inducibility of Atrial Fibrillation due to Stimulation of Ganglionated Plexi. Journal of Cardiovascular Electrophysiology January 2007;18(1):83–90. ISSN 1540-8167.

[14] Heidenreich EA, et al. Adaptive Macro Finite Elements for the Numerical Solution of Monodomain Equations in Cardiac Electrophysiology. Annals of Biomedical Engineering 2010;38(7):2331–2345.

[15] Bailón R, et al. A Robust Method for ECG-Based Estimation of the Respiratory Frequency during Stress Testing. IEEE transactions on bio medical engineering July 2006; 53(7):1273–1285. ISSN 0018-9294.

[16] Celotto C, et al. Relationship Between Atrial Oscillatory Acetylcholine Release Pattern and f-wave Frequency Modulation: a Computational and Experimental Study. In 2020 Computing in Cardiology. 2020; 1–4.

Address for correspondence:

Chiara Celotto
Universidad de Zaragoza, Campus Río Ebro, Edif.I+D, C/ Poeta Mariano Esquillor, s/n, 50018 Zaragoza
chiaracelotto@unizar.es